

Editorial preface to special issue: Paleoenvironmental changes along the Asian Continental margin over Neogene to recent timescales



Zhengquan Yao^{a,b,*}, Shuqing Qiao^{a,b}, Christophe Colin^c, Yusuke Okazaki^d, Yanguang Dou^e

^a Key Laboratory of Marine Geology and Metallogeny, First Institute of Oceanography, MNR, Qingdao, China

^b Laboratory for Marine Geology, Qingdao Marine Science and Technology Center, Qingdao, China

^c Université Paris-Saclay, CNRS, GEOPS, France

^d Kyushu University, Fukuoka, Japan

^e Qingdao Institute of Marine Geology, China Geological Survey, MNR, Qingdao, China

ARTICLE INFO

Editor: Howard Falcon-Lang

Keywords:

Asian Continental margin

Neogene

Paleoenvironment and Paleoclimate

Source-to-sink

ABSTRACT

The Asian Continental Margin, comprising the northeastern Arctic margin, the western Pacific margin, and the northeastern Indian Ocean margin, forms the most extensive continental margin system on Earth. To advance the understanding of paleoenvironmental and paleoclimatic changes of this important region, this Virtual Special Issue (VSI) entitled *Paleoenvironmental changes along the Asian Continental Margin over Neogene to recent timescales*, brings together fifty-two contributions that span a broad temporal range. The papers are grouped into four major themes that address the evolution of the Asian Continent Margin: (1) Sediment source-to-sink processes and multi-scale paleoenvironmental evolution; (2) Sedimentary environments and their linkages to tectonic, climatic, and sea-level changes; (3) Sedimentary processes in Arctic and subarctic marginal seas and their implications for oceanic, cryospheric, and atmospheric systems; and (4) Organic carbon burial and the global carbon cycle. Employing a wide array of methodologies, including sedimentology, geochemistry, paleontology, mineralogy, and climate modeling, this VSI addresses environmental changes from tectonic to millennial and centennial timescales. The findings, not only, offer critical insights into past climatic system evolution, but also provide a valuable basis for predicting the future response of marginal marine systems to ongoing global climate change.

1. Introduction

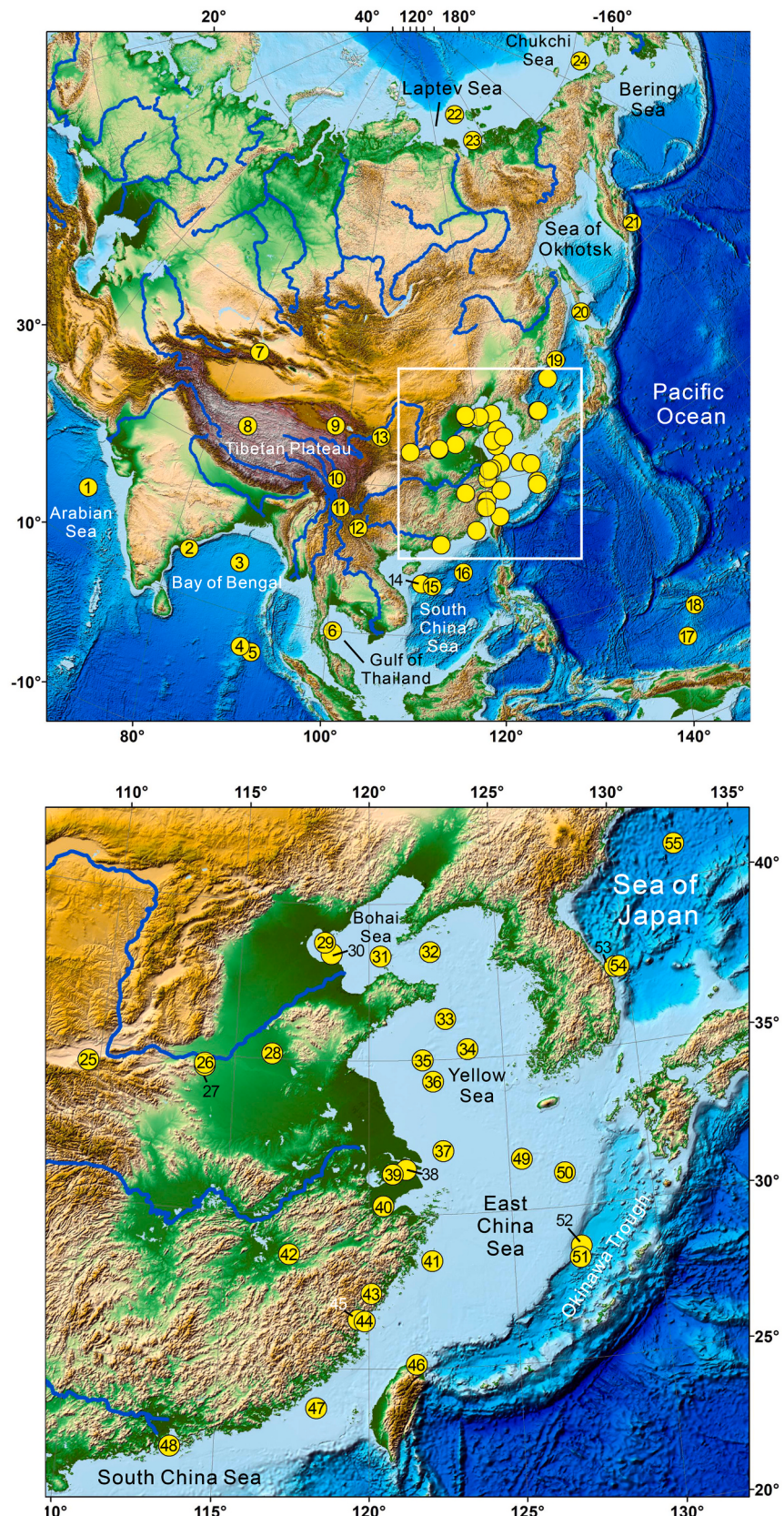
The Asian Continental Margin, comprising the northeastern Arctic margin, the western Pacific margin, and the northeastern Indian Ocean margin, forms the most extensive continental margin system on Earth. Positioned at the convergent boundaries of the Eurasian, Pacific, and Indo-Australian plates, it is one of the most tectonically dynamic regions. It also represents a critical interface between the Asian continent, the Pacific and Indian Oceans, where interactions between lithosphere, hydrosphere, cryosphere, and atmosphere are particularly intense. Over geological time, thick sedimentary sequences accumulated along these margins which preserve rich archives of land-ocean interactions, as well as paleoenvironmental and paleoclimatic evolution.

The vast geographical extent and geological complexity of the Asian continental margin mean it has been influenced by a range of global-scale processes operating over diverse temporal scales. These include the expansion and retreat of continental ice sheets (Dyke et al., 2002;

Jakobsson et al., 2014; Knies et al., 2001; Jakobsson et al., 2016), variations in sea-ice extent (de Vernal et al., 2020; Kinnard et al., 2011; Stein et al., 2017; Wang et al., 2021), changes in the strength and pattern of the Asian monsoon (An et al., 2015; Clemens et al., 1991; Clift et al., 2014; Prell and Kutzbach, 1987), and reorganization of ocean circulation (Ahagon et al., 2003; McManus et al., 2004; Rae et al., 2020; Gorbarenko et al., 2024). These processes have left an imprint not only on the sedimentary record but also on the biogeochemical and ecological systems of the region. Understanding the paleoenvironmental evolution of these margins is therefore vital for predicting future environmental change in response to ongoing global warming.

This Virtual Special Issue (VSI), entitled *Paleoenvironmental changes along the Asian Continental Margin over Neogene to recent timescales*, brings together new insights from sedimentological, geochemical, and modeling studies to explore the interactions between cryospheric, oceanic, and atmospheric systems over multiple timescales. There is a total of 52 articles in this VSI (Fig. 1, Table 1), and these research articles

* Corresponding author at: Key Laboratory of Marine Geology and Metallogeny, First Institute of Oceanography, MNR, Qingdao, China.
E-mail address: yaozq@fio.org.cn (Z. Yao).



(caption on next page)

Fig. 1. Map of Asian continental margin showing the location of study sites in this special issue. Numbers refer to the following articles in this special issue. 1) Thena et al. (2025); 2) Mohanty et al. (2025); 3) Li et al. (2024c); 4) Song et al. (2024); 5) Fernandes et al. (2025); 6) Bai et al. (2025); 7) Wang et al. (2024); 8) Li et al. (2024b); 9) Li et al. (2024d); 10) Li et al. (2025a); 11) Xu et al. (2025b); 12) Cao et al. (2024); 13) Niu et al. (2024); 14) Liang et al. (2025); 15) Wu et al. (2025); Ye et al. (2025); 16) Deemuenwai et al. (2025); 17) Dang et al. (2024); 18) Zheng et al. (2025); 19) Dou et al. (2025); 20) Razjigaeva et al. (2025); 21) Gorbarenko et al. (2025); 22) Li et al. (2025b); 24) Ye et al. (2024); 25) Xiao et al. (2025); 26) Zhang et al. (2025c); 28) Yuan et al. (2025); 29) Wu et al. (2024); 30) Liu et al. (2025); 31) Xiong et al. (2025); 32) Tang et al. (2025); 33) Zhang et al. (2025a); 34) Pi et al. (2024); 35) Du et al. (2025); 36) Li et al. (2024a); 37) Zhang et al. (2025b); 38) Yue et al. (2024); 39) Xu et al. (2024); 40) Zhang et al. (2025e); 41) Zhang et al. (2024); 42) Lu et al. (2025); 43) Liu et al. (2024); 44) Liu et al. (2024); 45) Rahman et al. (2025); 47) Zhang et al. (2025f); 48) Yu et al. (2025); 49) Cong et al. (2025); 51) Huang et al. (2025); 52) Xu et al. (2025a); 53) Novoselova et al. (2025); A record from the northeastern Pacific (Peng et al., 2025) is not shown on the map.

provide a comprehensive understanding of how the Asian continental margin has recorded and responded to global climate, offering valuable perspectives on both past and future Earth system dynamics.

2. Summary of special issue contributions

2.1. Sediment source-to-sink process and multi-scale paleoenvironmental evolution along the Asian Continent and its Margins

The sedimentary records from the Asian continental margin preserve evidence of source-to-sink processes and multi-scale paleoenvironmental evolution, providing critical geological insights into climate change since the Neogene. In this special issue, twenty-two articles focus on both terrestrial and marine sedimentary records from the Asian continental margin, with the goal of reconstructing the history and underlying mechanisms of climate evolution on tectonic, orbital, and millennial-to-centennial timescales since the Neogene.

Liang et al. (2025, this VSI) present a high-resolution cyclostratigraphic analysis of late Oligocene-early Miocene paleoclimate based on data from well Ls33a in the Qiongdongnan Basin. Using objective statistical methods, they identify astronomical signals and establish a 7.32-million-year floating timescale (28.55–21.23 Ma). Results show a muted sea-level response to orbital forcing near the Oligocene-Miocene boundary and identify three distinct climate stages based on sporopollen data. The study reveals phase shifts in climate responses attributed to local sedimentary nonlinearities and proposes a new conceptual model illustrating how obliquity modulates climate system dynamics in the northern South China Sea.

Ye et al. (2025, this VSI) examine unique anticline-shaped “hummocky” structures on the Xisha Islands as indicators of paleostorm activity during MIS 5. Through detailed sedimentological analysis and U-Th dating, they identify diagnostic features, including gentle dip angles (<5°), dominance of medium-grained carbonate sands, and hummocky cross-stratification. The study proposes two beach-ridge formation models: low-angle constructive ridges formed during cold periods and high-angle erosional features associated with warm phases. The results suggest that intense paleostorms occurred during MIS 5 warm intervals or transitions from cold to warm conditions, providing new insights into interglacial storm dynamics in the South China Sea.

Deemuenwai et al. (2025, this VSI) reconstruct early to middle Miocene deep-water circulation intensity in the South China Sea using sortable silt proxies from IODP Site U1500. Their analysis reveals a strong correlation between mean sortable silt size and its percentage, validating the proxy's reliability. Results indicate enhanced Lower Circumpolar Deep Water during 23–20 Ma, followed by a marked decline in intensity associated with basin expansion between 20 and 16 Ma. The study highlights the combined tectonic and oceanographic influences on the evolution of deep-water circulation in the region.

Dang et al. (2024, this VSI) investigate the evolution of upper-water structure in the Western Pacific Warm Pool (WPWP) over the past 4 Ma using planktonic foraminifera $\delta^{18}\text{O}$ and $\delta^{13}\text{C}$ records from IODP Site U1489. Their results reveal progressive thermocline shoaling and a decline in respired carbon content since the Pliocene, suggesting increased vertical mixing and a contraction of the circulation cell. The study identifies two major transitional intervals at ~3.1 Ma and ~0.7 Ma, marking the development of modern WPWP characteristics. Their

findings provide new constraints on tropical Pacific circulation dynamics in response to late Cenozoic climate cooling.

Zheng et al. (2025, this VSI) investigate late Neogene Asian dust input to the western Pacific using grain-size distributions and Sr–Nd isotopic compositions of the <4 μm fraction from IODP Site U1490. Through Weibull function analysis, they identify EM2 as a dust population originating from northern Chinese deserts, transported by the East Asian winter monsoon and westerlies. Results show coarser EM2 modes during 7.2–4.8 Ma and 3.9–2.6 Ma, coinciding with southward shifts of the Intertropical Convergence Zone (ITCZ) and the intensified Asian aridification. The research highlights the role of ITCZ migration in modulating dust deposition patterns in the low-latitude western Pacific, independent of climatic changes in the dust source regions.

Rahman et al. (2025, this VSI) reconstruct hydroclimate variability over the past 13.3 ka from sediment cores (TTV-11/17) in Tsui Tsui Valley. Diatom assemblages and micro-XRF geochemistry reveal predominantly lacustrine conditions between 11.1 and 8.8 ka BP, punctuated by episodic runoff events. Principal component analysis links detrital elements to monsoon variability: dry conditions from 13.3 to 8.0 ka BP are associated with a strengthened East Asian Winter Monsoon, while wetter phases from 4.5 to 0.2 ka BP reflect intensification of the East Asian Summer Monsoon under La Niña-like conditions. The study highlights climatic teleconnections between subtropical East Asia and high latitude (Arctic ice, Atlantic Meridional Overturning Circulation) and tropical El Niño-Southern Oscillation (ENSO) climate systems.

Huang et al. (2025, this VSI) examine authigenic eNd records from core Oki01 in the Okinawa Trough to trace water mass evolution. Over the past 6 ka BP, eNd variations reflect the mixing of North Pacific Intermediate Water and South China Sea Intermediate Water. During 16–10 ka BP, more unradiogenic eNd values correspond with intensified monsoon precipitation and increased riverine input of pedogenic minerals from the Changjiang and Huanghe catchments. The study demonstrates that continental weathering products can significantly influence seawater eNd signatures, adding complexity to the interpretation of paleocirculation in marginal seas.

Pi et al. (2024, this VSI) reconstruct the evolution of the Yellow Sea Warm Current (YSWC) and Cold Water Mass (YSCWM) since 6 ka using grain-size end-member analysis and benthic foraminiferal assemblages from 37 surface sediment samples and core Z1 in the Yellow Sea. The YSWC underwent three main phases: rapid intensification (6.0–3.9 ka), a decline to modern levels (3.9–1.9 ka), and a relatively stable period (1.9–0.0 ka), with brief strengthening events at 1.4 ka and 0.3 ka. The YSCWM exhibited synchronous variability with the YSWC, except during key intervals around 4.0–3.9 ka, ~2.5 and 2.0 ka. The study highlights the greater sensitivity of the YSCWM to ENSO variability, suggesting it is a more reliable proxy for reconstructing the palaeoceanographic conditions in the Yellow Sea.

Cong et al. (2025, this VSI) investigate climate-driven sedimentation in the southwestern Cheju Island Mud area (SWCIM). Analysis of heavy and clay minerals, along with benthic foraminifera, reveals that sediments from the Yangtze and Yellow Rivers have been transported to the region by the Yellow Sea Coastal Current (YSCC) and Yellow Sea Warm Current (YSWC) since 8.2 ka. Sediment supply was primarily modulated by the East Asian monsoon and ENSO variability, while changes in current strength affected the efficiency of the regional vortex system,

Table 1

Summary of study area, sites, age/period, and method/proxy in the Virtual Special Issue.

Site No.	Site name	Study area	Age/period	Method/proxy	References
1	U1457	Laxmi Basin, Arabian Sea	~10.8 Ma	Foraminiferal analysis	Thena et al., 2025
2	NGHP-15 A	Bay of Bengal	~1300 yr	AMS ^{14}C dating, planktic foraminifera analysis	Mohanty et al., 2025
3	BOB-56	Bay of Bengal	~42 ka	Element composition, Nd isotope	Li et al., 2024c
4	Site 758	Bay of Bengal	~30 Ma	REE, Nd—Pb isotope	Song et al., 2024
5	MGS 22/01	Bay of Bengal	~55 ka	AMS ^{14}C dating, TOC, TN, $\delta^{13}\text{C}$, $\delta^{15}\text{N}$, element composition	Fernandes et al., 2025
6	T93	Gulf of Thailand	~16.3 ka	AMS ^{14}C dating, grain size, TOC, TN, $\delta^{13}\text{C}$, n-alkanes	Bai et al., 2025
7	TLD16	Yili valley	~60 ka	AMS ^{14}C dating, OSL dating	Wang et al., 2024
8	Amdo section	Qiangtang Basin	~166–144 Ma	CL, SEM, element composition, $\delta^{13}\text{C}$, $\delta^{18}\text{O}$	Li et al., 2024b
9	Wulan	Northeastern Tibetan Plateau	~18 Ma	pollen analysis	Li et al., 2024d
10	CW	Southeastern Tibetan Plateau	~140 ka	OSL dating, Magnetic susceptibility, color reflectance, grain size	Li et al., 2025a
11	Heqing drill core	Heqing Basin	~130 ka	magnetic analysis (ARM/SIRM)	Xu et al., 2025b
12	Qilu	Lake Qilu	~15 ka	AMS ^{14}C dating, XRF, n-alkane analysis	Cao et al., 2024
13	Huinling	Huinling Loess	~2 Ma	Detrital zircon U—Pb dating	Niu et al., 2024
14	LS33a	South China Sea	Oligocene to Miocene	planktic foraminiferal and sporopollen analysis	Liang et al., 2025
15	XK-1	South China Sea	~11 Ma	sedimentological and paleontological analysis	Wu et al., 2025
16	U1500	South China Sea	~24 Ma	Grain size, foraminifera analysis	Ye et al., 2025
17	U1489	Western Pacific warm pool	~4 Ma	Grain size, carbonate analysis	Deemuenwai et al., 2025
18	U1490	Western Pacific warm pool	~8.6 Ma	Planktonic foraminifera isotope analyses	Dang et al., 2024
19	LV53-18-2	Sea of Japan	~21 ka	Grain size, Sr and Nd isotopes	Zheng et al., 2025
20	Peat bog	Sakhalin Island	~6 ka	Grain Size, element composition, clay minerals	Dou et al., 2025
21	LV63-41-2	Southeastern Kamchatka	~21 ka	Ash content, diatom analysis	Razjigaeva et al., 2025
22	LV83-16-1	Laptev Sea	~12 ka	AMS ^{14}C dating, magnetic susceptibility, $\delta^{13}\text{C}$, C/N, diatom analysis	Gorbarenko et al., 2025
23	LV83-32-3			benthic foraminiferal analysis, pollen analyses	Li et al., 2025b
24	LV77-3	Chukchi Shelf margin	~10 ka	AMS ^{14}C dating, element composition, $\delta^{13}\text{C}$, grain size	Ye et al., 2024
25	GT3	Weihai Basin	~3.5 Ma	TOC, $\delta^{13}\text{C}$	Xiao et al., 2025
26	BS	Eastern Henan Basin	~3.6 Ma	Paleomagnetic dating, Magnetic susceptibility, Grain size	Zhang et al., 2025c
27	HKG			Element composition	
28	JZK5	Shandong Plain	~123 ka	OSL dating	Yuan et al., 2025
29	DZQ01	Bohai Sea	~300 ka	Grain size, trace element, AMS ^{14}C dating, OSL dating	Wu et al., 2024
30	BHB1	Bohai Sea	~14 ka	AMS ^{14}C dating, grain size, TOC, TN, $\delta^{13}\text{C}$, $\delta^{15}\text{N}$	Liu et al., 2025
31	CSH05	Bohai Sea	~2.3 Ma	Paleomagnetic measurements, foraminifera analysis, OSL dating, grain size	Xiong et al., 2025
32	DLC70-2	Yellow Sea	~240 ka	OSL dating	Tang et al., 2025
33	YS-A	Yellow Sea	~7 ka	AMS ^{14}C dating, grain Size, black carbon, polycyclic aromatic hydrocarbons	Zhang et al., 2025a
34	Z1	Yellow Sea	~6 ka	Grain size, benthic foraminifera analysis	Pi et al., 2024
35	C02	Yellow Sea	~11.5 ka	Carbonate analysis, $\delta^{13}\text{C}$, $\delta^{18}\text{O}$	Du et al., 2025
36	CSDP-2	Yellow Sea	~4 Ma	Nd isotope, clay minerals	Li et al., 2024a
37	CRE-1402	Yangtze (Changjiang) River Shoal	~140 ka	Detrital heavy and light minerals	Zhang et al., 2025b
38	LQ19-176 m	Yangtze (Changjiang) River Delta	Pliocene	Detrital zircon U—Pb dating	Yue et al., 2024
39	CJK11	Yangtze (Changjiang) River Estuary	~4 ka	Trace elements, strontium isotope, clay minerals	Xu et al., 2024
40	SE3	Qiantang River	~14 ka	Grain size, trace element, TOC, TN	Zhang et al., 2025e
41	ECMZ	East China Sea	~18 ka	TOC, TN, $\delta^{13}\text{C}$	Zhang et al., 2024
42	Shennong Cave	Southeastern China	~11 ka	^{230}Th dating, $\delta^{13}\text{C}$, $\delta^{18}\text{O}$	Lu et al., 2025
43	NDQK11	Ningde Bay	~140 ka	element composition, OSL and AMS ^{14}C dating	Liu et al., 2024
44	NDGK73				
45	NDGK2				
46	TTV-11/17	Taiwan Tsui Tsui Valley	~13.3 ka	AMS ^{14}C and ^{210}Pb dating, XRF, diatom analysis, C—N contents, $\delta^{13}\text{C}$	Rahman et al., 2025
47	ZK01	Taiwan Strait	~3.6 Ma	AMS ^{14}C and OSL dating, Paleomagnetic analysis, grain-size, color reflectance	Zhang et al., 2025f
48	MAC18QZ01	Pearl River estuary, China	Late Pleistocene	AMS ^{14}C dating, pollen analysis, foraminifera and ostracoda analysis, grain size	Yu et al., 2025
49	Z7	East China Sea	~8.2 ka	AMS ^{14}C dating, grain size, heavy minerals, clay minerals, benthic foraminiferal analysis	Cong et al., 2025
50	ZB8			REE, Sr—Nd isotopes	
51	Oki01	Okinawa Trough	~16 ka	AMS ^{14}C dating, grain size, element composition	Huang et al., 2025
52	C01	Okinawa Trough	~20 ka	AMS ^{14}C dating, grain size, element composition	Xu et al., 2025a
53	05GCRP-13	Sea of Japan	~70 ka	AMS ^{14}C dating, TOC, TS, biogenic opal, $\delta^{13}\text{C}$, $\delta^{18}\text{O}$, element composition, Nd isotope	Jang et al., 2025
54	05GCRP-14			pollen analysis	
55	LV 53-27-1	Sea of Japan	~120 ka		Novoselova et al., 2025

(continued on next page)

resulting in shifts of the sediment depocenter. This study establishes the SWCIM as a valuable archive of ocean-climate-sediment interactions, offering implications to predict future marine environmental changes.

[Peng et al. \(2025, this VSI\)](#) investigate carbonate production from the middle Pleistocene to the Holocene in the Guaymas Basin using CaCO_3 content from IODP Site U1546. A refined age model is established and 12 marine isotope stages are identified, revealing elevated carbonate accumulation during the interglacials. However, carbonate production was constrained by diatom dominance and organic matter remineralization under eutrophic conditions. The study provides important data for Pacific-wide comparisons of climate-carbonate system interactions and highlights coccolithophore temperature preferences as the primary control on carbonate accumulation patterns.

[Thena et al. \(2025, this VSI\)](#) investigate benthic foraminiferal responses to Late Miocene (~11–9 Ma) mass transport deposits (MTDs) in the Laxmi Basin, Arabian Sea, using data from IODP Site U1457. The MTDs, composed of mixed carbonate breccias and Indus-derived sediments, are associated with reduced foraminiferal diversity and evidence of dysoxic conditions. Declines in characteristic taxa are attributed to changes in sediment texture and variations in organic matter, while species adapted to oxygen-minimum zones appear fragmented. Diversity indices indicate a gradual post-MTD recovery, following ecological succession patterns. This study provides critical insights into benthic ecosystem resilience to large-scale submarine slope failures, highlighting how such depositional events reshape microhabitats and trophic dynamics in deep-sea settings over millennial timescales.

[Zhang et al. \(2025d, this VSI\)](#) investigate the solar modulation of eastern China hydroclimate patterns (ECHPs) under the combined influences of the Pacific Decadal Oscillation (PDO) and Atlantic Multidecadal Oscillation (AMO) using Community Earth System Model simulations. Under strong solar forcing, positive AMO/PDO phases induce meridional dipole patterns via Eurasian teleconnections, whereas weak solar activity leads to a reversal pattern. The study also identifies tripole ECHPs associated with negative PDO and positive AMO phases, with vertical moisture transport playing a key role in shaping all scenarios. These findings enhance our understanding and predictive capacity of monsoon rainfall variability under varying ocean-atmosphere conditions.

[Yue et al. \(2024, this VSI\)](#) use detrital zircon geochronology to study provenance shifts in the Yangtze Delta since the Pliocene. Pliocene sediments show age peaks between 100 and 200 Ma, consistent with input from nearby local rivers, indicating a confined pre-Quaternary paleo-Yangtze system. Pleistocene deposits display a broader range of zircon ages (11.9–3643 Ma), reflecting the incorporation of sediments from the upper-middle Yangtze River, including the Cenozoic zircons derived from the Tibetan Plateau after ~1.6 Ma. These findings document the delta's evolution from an intermontane basin to an alluvial-fluvial plain, driven by tectonic subsidence and river integration across eastern China.

[Cao et al. \(2024, this VSI\)](#) explore ecological changes at Lake Qilu in southwestern China since 14.6 cal ka BP using n-alkane proxy. Variations in short-, mid-, and long-chain n-alkanes reveal distinct vegetation phases. From 14.6 to 6 cal ka BP, warm and humid conditions supported abundant aquatic and terrestrial plants. Between 6 and 2 cal ka BP, aquatic plants flourished due to human activities. After 2 cal ka BP, bacteria and algae increased, resulting from anthropogenic eutrophication. The study demonstrates a clear transition from climate-dominated to human-driven ecological change at ~6 ka, highlighting

the growing influence of anthropogenic forcing on lake ecosystems during the Holocene.

[Li et al. \(2024b, this VSI\)](#) reconstruct the Late Jurassic paleoclimate in the Qiangtang Basin using bulk carbonate $\delta^{18}\text{O}$ and $\delta^{13}\text{C}$. The $\delta^{18}\text{O}$ data reveal a cooling trend across the Callovian-Oxfordian transition, followed by mid-Oxfordian warming and subsequent Late Oxfordian cooling. These climatic shifts are closely linked to sea-level and CO_2 changes. Positive $\delta^{13}\text{C}$ excursions correspond to periods of enhanced weathering and productivity during warm intervals, whereas cooling phases show reduced organic carbon burial. This study validates the bulk carbonates as reliable paleotemperature proxies in the absence of well-preserved biogenic material, providing new insights into Jurassic climate dynamics in the eastern Tethys region.

[Li et al. \(2024d, this VSI\)](#) examine the Miocene palynological assemblages from the Wulan Basin to explore the relationship between climate change and Tibetan Plateau (TP) uplift. The pollen record is divided into four pollen zones, all dominated by shrub-grass, suggesting an altitudinal zonation pattern. Coexistence Likelihood Estimation analysis indicates mean annual temperatures of 6.0–14.7 °C and precipitation of 919–1612 mm during the Miocene, a period significantly warmer/humid than modern conditions. Paleoelevation estimates of 1655–2025 m imply an uplift of 1275–1645 m. These results support regional models of phased TP uplift and its climatic consequences.

[Li et al. \(2025a, this VSI\)](#) reconstruct Indian Summer Monsoon (ISM) variability over the past ~135 ka using the Cuoweng loess-paleosol sequence from southeastern Tibet. The record reveals pronounced glacial-interglacial fluctuations in ISM during the last glacial cycle. Suborbital-scale variations are especially evident in MIS 5, with strengthened monsoon during MIS 5a, 5c, and 5e, and weaker phases during MIS 5b and 5d. The results suggest that ISM variability was driven by a combination of high- and low-latitude forcing. This high-resolution record provides valuable information on monsoon dynamics on the Tibetan Plateau during the last glacial cycle.

[Wang et al. \(2024, this VSI\)](#) address radiocarbon age underestimation in arid Central Asian loess by comparing ^{14}C with optically stimulated luminescence (OSL) ages from the TLD16 section in the Yili valley. All radiocarbon samples consistently yield younger ages than their OSL counterparts, with root contamination identified as the primary cause of this discrepancy. Comparative regional data show that this age bias is more pronounced in arid regions than in monsoon-dominated areas. The study underscores the limitations of relying solely on ^{14}C dating for pre-Holocene loess in drylands and emphasizes the necessity of multi-method chronological validation for robust age control.

[Xu et al. \(2025b, this VSI\)](#) explore the linkages between the Indian Summer Monsoon (ISM) and the Atlantic Meridional Overturning Circulation (AMOC) using magnetic proxies (ARM/SIRM) from the Heqing drill core in southwestern China. The results show that orbital-scale ISM variability was synchronized with AMOC intensity, both pacing precession cycles. Observed phase lags between ISM precipitation and insolation are attributed to cumulative delays arising from ITCZ-AMOC interactions. This study provides compelling evidence for teleconnections between monsoon intensity and Atlantic circulation during the late Pleistocene.

[Niu et al. \(2024, this VSI\)](#) investigate Quaternary loess provenance changes in the western Chinese Loess Plateau (CLP) using detrital zircon U–Pb dating of 12 loess layers. The results show a dominant sediment source shift from the northeastern Tibetan Plateau (NTP, 1.8–1.66 Ma) to the Gobi Altay Mountains (GAMs, 1.5–1.4 Ma), followed by an abrupt

Table 1 (continued)

Site No.	Site name	Study area	Age/period	Method/proxy	References
/	U1546	Guaymas Basin, Eastern Pacific Ocean	~450 ka	Carbonate analysis	Peng et al., 2025
/	/	Eastern China	~2 ka	Community Earth System Model	Zhang et al., 2025d

return to NTP after 1.24 Ma. These provenance transitions correspond to episodes of Tibetan uplift and the Kunhuang Movement, demonstrating the combined influence of tectonics and climate on dust transport via the East Asian winter monsoon. The study provides crucial constraints on the coupling between Tibetan Plateau uplift and downwind aeolian depositional systems.

Xiao et al. (2025, this VSI) reconstruct the evolution of the Weihe Basin since the late Pliocene based on paleomagnetic and sedimentological data from core GT3. The basin evolution is divided into four stages: shallow lacustrine (3.69–2.58 Ma), fluvial (2.58–1.8 Ma), alternating fluvial-aeolian (1.8–1.3 Ma), and arid settings (post-1.3 Ma). The establishment of modern drainage patterns during the early Pleistocene suggests that the Yellow River integration through Sanmenxia Gorge occurred by ~1.3 Ma. This study resolves long-standing debates on the timing of the Yellow River's transition from an endorheic to exorheic system, linking this hydrological shift to regional tectonic subsidence.

Zhang et al. (2025c, this VSI) present high-resolution elemental records from fluvial sequences in the eastern Henan Basin, capturing hydroclimate fluctuations over the past 3.5 Ma. Multivariate analysis of ten elements reveals that the first principal component (PC1) reflects summer monsoon hydrodynamics, while PC2 tracks dry-wet climate cycles. Three distinct climate stages are identified: a humid late Pliocene (3.5–2.8 Ma), a drier early Pleistocene (2.8–0.9 Ma), and a humid late Pleistocene (post 0.9 Ma). These results document the stepwise evolution of the East Asian Summer Monsoon and provide a terrestrial counterpart to marine and speleothem monsoon proxies.

2.2. Sedimentary environments of the Asian Continental Margin and their linkages to tectonic, climatic, and sea-level changes

Due to its unique geographic setting, the Asian continental margin has been profoundly influenced by tectonic activity, climate variability, and sea-level changes throughout geological time. The following twenty articles focus on sedimentary records from the marginal seas of the northwest Pacific, the coastal regions off eastern China, and the north-eastern Indian Ocean. These studies collectively aim to reconstruct the evolution of sedimentary environments along the Asian continental margin since the Neogene and to elucidate their linkages to tectonic processes, climate change, particularly the Asian monsoon, and sea-level fluctuations.

Yu et al. (2025, this VSI) investigate late Pleistocene vegetation and climate changes in the Pearl River Estuary through analyses of pollen, foraminifera, and ostracoda from sediment cores off the Macau Sea. By integrating AMS ^{14}C and OSL dating with microfossil data, they establish a robust chronostratigraphic framework. The results indicate that mangrove and tropical rainforest elements during MIS 5 reflect warm conditions comparable to the early Holocene (9.2–7.5 ka BP). The study further identifies extensive mud tidal flats during MIS 5 and documents significant anthropogenic impacts over the last 900 years. These findings provide important records of late Quaternary marine cycles in a subtropical estuarine system.

Wu et al. (2025, this VSI) examine the evolution of the Late Miocene carbonate system in the Xisha area based on detailed sedimentological and paleontological analyses of core XK-1. Their study reveals an early Late Miocene alternation between patch reef and lagoonal bioclastic deposits, which later transitioned to predominantly lagoonal facies. A gradual expansion of reef development during the early Late Miocene is attributed to eustatic sea-level fall. The dominance of red algae, Halimeda, and bryozoans after ~7.1 Ma indicates increased nutrient availability, likely linked to intensified East Asian Winter Monsoon-driven upwelling. These findings highlight the combined influence of sea level, tectonics and monsoonal variability on the development of carbonate systems in the South China Sea.

Xu et al. (2024, this VSI) reconstruct the Holocene evolution of the subaqueous Changjiang Delta based on analyses of core CJK11. Analyses of clay minerals, trace elements, and $^{87}\text{Sr}/^{86}\text{Sr}$ ratios reveal significant

sediment contributions from both the Yellow River and the Changjiang River. Three evolutionary stages are identified: (1) slow neritic sediment accumulation from 10 to 5 ka; (2) a depositional hiatus between 5 and 3 ka under cold/arid conditions; (3) prodelta formation from 3 ka to present, marked by spatially variable fluvial inputs. The study highlights the roles of climate variability, Yellow River channel migration, and coastal current processes in shaping the delta's sedimentary history.

Zhang et al. (2025b, this VSI) analyze mineral assemblages of core CRE-1402 from the Yangtze Shoal to reconstruct estuary dynamics since MIS 6. Both light and heavy mineral compositions resemble sediments from the lower Yangtze River and adjacent offshore areas. Stable hornblende-to-epidote ratios and garnet-to-epidote ratios indicate a consistent terrigenous sediment source. Quartz–Feldspar–Lithics ternary plots confirm Yangtze River dominance, with evidence for channel migration in response to sea-level fluctuations: during low sea levels in MIS 6, the Yangtze River flowed through the study area; from MIS 5 to MIS 2, it shifted to other regions; and during the high sea levels of MIS 1, the river migrated south of the core site. The study clarifies the formation of the shoal as a result of the dynamics of fluvial-marine interactions.

Liu et al. (2024, this VSI) examine sediment source-to-sink processes along the southeastern coast of China based on late Quaternary deposits from the Ningde Bay. Using OSL dating and geochemical analyses, they identify alternating sediment provenance from the Yangtze River during MIS 5e, 3, and 1, and from local sources during MIS 4. Notably, fine-grained quartz in MIS 3 yields older OSL ages (90–140 ka) compared to medium-grained quartz (40–80 ka), indicating the reworking and redeposition of older Yangtze-derived offshore sediments under weakened East Asian monsoon. This study proposes a new compensation model in which diminished Yangtze River input triggers offshore sediment recycling, offering new insights into the response mechanisms of the distal sedimentary system to fluctuations in fluvial sediment supply.

Zhang et al. (2025e, this VSI) employ grain-size end-member (EM) modeling to core SE3 from the Qiantang River to decipher the influence of sea-level and climate impacts on coastal sedimentation since the Last Glacial Maximum. The proportion of the finest EM1 and the combined abundance of the coarsest EMs (i.e., EM5 + EM4) exhibit clear sensitivity to relative sea-level variations. Vertical variations in grain-size data mainly reflect the combination of the Zhe-Min coastal currents and intermittently strengthening East Asian Winter Monsoon. In addition, three paleoflood intervals are identified via EM5 peaks, demonstrating coastal system sensitivity to abrupt climate events.

Zhang et al. (2025f, this VSI) analyze a 160-m sediment core (ZK01) to reconstruct the sedimentary history of the Taiwan Strait over the past ~4 Ma. Magnetostratigraphic data indicate a relatively stable sedimentation rate before 1.07 Ma, followed by a doubling of accumulation during 1.07–0.77 Ma, likely driven by regional tectonic activity and climatic variability during the Mid-Pleistocene Transition (MPT). Grain-size and color proxies reveal sea-level fluctuations, while the presence of thinner sediment units after the MPT indicates regional tectonic uplift. In contrast to the Yellow and Bohai seas, these findings demonstrate a distinct history of subsidence-uplift in the strait, providing new insights into marginal sea evolution under the combined influence of tectonics and climate.

Xu et al. (2025a, this VSI) trace sediment provenance changes in Okinawa Trough using core C01 since 19 cal. ka BP. AMS ^{14}C dating and geochemical data show that the Changjiang River dominated sediment supply during the last glacial lowstand (19.0–11.3 ka BP). With post-glacial sea-level rise (11.3–7.3 ka BP), sediment provenance shifted to a mixed contribution from the Changjiang and Taiwan sources. The intensification of the Kuroshio Current (KC) is found to be linked to variations in Northern Hemisphere summer insolation and the strength of the East Asian Winter Monsoon. Volcanic inputs at 7.3 ka BP and ENSO-driven KC weakening at 4.9 ka BP further modified sediment composition, reflecting the influence of both regional tectonic and low-latitude Pacific climate.

Liu et al. (2025, this VSI) investigate transgressive deposits in the western Bohai Sea through analysis of borehole BHB1, focusing on the development of peat beds during the mid-Holocene. The sedimentary sequence reveals alternating peat layers and coastal muds formed between 7 and 5 ka BP under fluctuating waterlogged and oxidizing conditions. These intervals coincide with intensified East Asian Summer Monsoon, elevated summer insolation, and climate warming. Peat accumulation ceased around 7 ka BP, likely due to increased Yellow River sediment input associated with delta progradation. The findings highlight the coupled influence of monsoonal climate and fluvial sediment supply on the formation of a unique backstepping aggradational system, providing new insights into the mechanism driving coastal peat formation.

Xiong et al. (2025, this VSI) examine the sedimentary core CSH05 from the Bohai Sea to reconstruct Quaternary transgression history. The core reveals 13 sedimentary units characterized by alternating marine and terrestrial deposits over the past 1.35 Ma. The earliest identified transgression (U13) occurred no later than 1.35 Ma, with complete marine inundation of the basin achieved after 0.3 Ma, due to the full subsidence of the Miaodao Islands uplift. Neritic deposits layer during MIS 3 show weaker transgression compared to those of MIS5 and MIS1. This study integrates tectonic (Tibetan uplift), climatic (glacial cycles), and fluvial (Yellow River) factors in a new model for the transgressive evolution of the Bohai and Yellow Sea.

Wu et al. (2024, this VSI) examine the development of Mid-Pleistocene paleochannels in the western Bohai Sea using core DZQ01. End-member modeling of grain size identifies two components that represent East Asian summer monsoon (EASM, EM3) and East Asian winter monsoon (EAWM, EM2), respectively. Five glacial events are recorded, among which DU6 (300–272 ka) and DU4 (165–127 ka) are marked by weakened EASM and/or stronger EAWM, while DU2 (71–14 ka) reflects a prolonged phase of EAWM dominance. The study highlights the influence of Tibetan Plateau uplift and sea-level fluctuations on channel formation through modulating monsoon intensity.

Tang et al. (2025, this VSI) establish a robust late Quaternary chronology for core DLC70-2in in the northern Yellow Sea using quartz OSL and feldspar pIRIR dating. Three transgressive layers are identified: T1 (MIS 1, 4.9–10.3 ka), T2 (MIS 5, 76 ± 7 ka), and T3 (MIS 7, 191 ± 17 ka). The study reveals a significant underestimation of ^{14}C age in pre-Holocene sediments. They also reconstruct a comprehensive late Quaternary stratigraphy using ten cores obtained from the Bohai Sea and Yellow Sea. This robust chronostratigraphic framework enables correlation across cores from the Bohai and Yellow seas, advancing our understanding of regional paleoenvironmental changes.

Li et al. (2024a, this VSI) study Plio-Pleistocene silicate weathering intensity along the East Asian continental margin using a multi-proxy approach, including Nd isotopes, detrital zircon ages, and Chemical Index of Alteration (CIA) data from core CSDP-2 in the Yellow Sea. A pronounced shift in ϵNd values from -18.8 (pre-3.6 Ma) to -11.3 (post-1.0 Ma), together with zircon age data, indicates that a modern-like Yellow River drainage system was fully established by the early Pleistocene. The CIA records show a more substantial decline in weathering intensity compared to other Asian regions, likely driven by the combined effects of large-river integration and global cooling. These findings emphasize the importance of considering source-to-sink system evolution when interpreting weathering signals in the continental margins.

Du et al. (2025, this VSI) investigate Holocene variation in carbonate content from sediment core C02 in the southern Yellow Sea. By integrating benthic foraminiferal abundances, detrital mineral compositions, and stable carbon and oxygen isotopes three phases are identified: stage III (11.2–10.1 ka BP) is characterized by high carbonate content (~80 %) in the <38 μm fraction, indicating offshore marine conditions; stage II (10.1–6.5 ka BP) shows a decline in fine-grained carbonate (60 %) and increased Yangtze River influence; stage I (6.5–4 ka BP) marks the establishment of the modern circulation regime.

Song et al. (2024, this VSI) examine the timing of the Himalayan

uplift through the analysis of marine sediments from ODP Site 758 in the Bay of Bengal. Using an Nd–Pb isotope mixing model, they demonstrate that Himalayan rivers became the dominant sediment sources starting ~23 Ma, with a progressive eastward expansion during the Miocene. The study suggests that major uplift of the Himalayas did not begin earlier than this time, and that near-modern elevations were likely reached by the late Miocene. This study provides important constraints on the tectonic evolution of the Himalayas through sediment fingerprinting techniques.

Fernandes et al. (2025, this VSI) examine the sources of organic matter and productivity variation in the southeastern Bay of Bengal over the past 54,000 years, based on sediment core MGS 22/01. Their multi-proxy approach reveals a dominance of terrestrial organic matter prior to ~15 ka BP, controlled by sea-level and Indian summer monsoon (ISM) variability. Redox-sensitive Mn/Al ratios indicate persistent oxic conditions between 12 and 6 ka BP, while peaks in productivity occurred during early MIS3, LGM, and the mid-late Holocene. This study provides key paleoproductivity data from a previously underexplored region, offering new insights into monsoon-driven biogeochemical cycling in the southern Bay of Bengal.

Li et al. (2024c, this VSI) reconstruct the erosion history of the Himalayan Mountain using sedimentary core BOB-56 from the Bay of Bengal. Elemental and mineralogical proxies show intensified chemical weathering during interstadials, closely aligned with Indian summer monsoon strength and sea surface temperature variability. The erosion signals from the Ganges-Brahmaputra system are transmitted rapidly to the marine archives without noticeable time lag on the millennial timescale. This study demonstrates the sensitivity of Himalayan erosion to abrupt climate shifts and suggests that monsoon-driven silicate weathering may have acted as a short-term carbon sink.

Mohanty et al. (2025, this VSI) reconstruct late Holocene paleceanographic and paleoenvironmental changes using planktic foraminifera from core NGHP-15 A in the western Bay of Bengal. Four climatic regimes are identified: oligotrophic conditions during the Roman Warm Period and Medieval Climate Anomaly due to intensified southwest monsoon and associated river discharge, and eutrophic conditions during the Dark Age Cold Period and the Medieval Climate Anomaly-Little Ice Age transition caused by strengthened northeast monsoon winds. The study links productivity changes to the Indian monsoon, demonstrating centennial-scale ecosystem responses to shifts in atmospheric circulation.

Yuan et al. (2025, this VSI) use OSL dating of Holocene sediments from Jining on the Yellow River Plain to identify three major hiatuses (0.48–1.31 ka, 2.66–4.41 ka, 5.20–47.7 ka), attributed to river avulsion events. Floodplain sedimentation has been episodic, marked by alternating flood and lacustrine deposits since 5.2 ka. Lacustrine phases at ~4 ka, 2–2.5 ka, and 1 ka correspond to known Yellow River course changes. The study underscores the discontinuous nature of floodplain records and highlights the importance of recognizing event-driven sedimentation in paleoenvironmental reconstruction.

Lu et al. (2025, this VSI) investigate Neolithic cultural transitions in southern Hangzhou Bay by correlating them with speleothem $\delta^{13}\text{C}$ and $\delta^{18}\text{O}$ records from Shennong Cave during the early and mid-Holocene. The Shangshan culture thrived under warm and wet conditions but declined following a drying event around 9.2–8.2 ka BP. The decline of the Kuahuqiao culture coincides with 240-year pluvial events (8.2–7.0 ka BP), while interruptions in the Hemudu culture may reflect flood disturbances under a persistently wet climate. The high-resolution record challenges deterministic interpretations of climate-culture relationships, while providing refined chronological context for early agricultural development.

2.3. Sedimentary processes in Arctic and subarctic Pacific marginal seas and their implications for oceanic, cryospheric, and atmospheric systems

The sedimentation in the Arctic and sub-Arctic Pacific is influenced

by a complex interplay of ice sheets/sea ice, ocean circulation, and atmospheric systems such as the westerlies and monsoons. This tightly coupled ocean-ice-atmosphere system in this region plays a critical role in regulating both regional and global climate dynamics. In this special issue, six articles focus on sedimentary records from the Arctic Ocean and the marginal seas of the northwest Pacific, exploring sedimentary processes and their linkages to ocean-ice-atmosphere interactions during the Late Quaternary.

[Dou et al. \(2025, this VSI\)](#) examine hydrodynamic changes in the Sea of Japan (JS) during the last deglaciation using sortable silt data from three sediment cores. The results reveal intensified currents in the southwestern JS at 18 ka, coinciding with the initial intrusion of the Tsushima Warm Current (TWC). By 16 ka, enhanced vertical mixing in the central JS was driven by the continued TWC inflow and the subpolar front migration. In contrast, hydrodynamic conditions in the northwestern JS were primarily influenced by brine rejection associated with sea-ice activity. The study highlights how TWC and sea-ice jointly drove regional oceanic variability.

[Novoselova et al. \(2025, this VSI\)](#) present a 120-ka pollen record from core LV 53–27-1 in the Sea of Japan to reconstruct vegetation and climate changes in northeast Asia. The record shows that oak-dominated forests prevailed during warm Dansgaard-Oeschger events (DOIs 24–8), corresponding to a strengthened East Asian Summer Monsoon (EASM) and high productivity. In contrast, cold Heinrich stadials were characterized by alder and birch shrubs, weakened EASM, and low productivity. The study reveals land-sea linkage and provides a continuous paleoenvironmental sequence in the Russian Far East, significantly advancing our understanding of regional ecosystem responses to abrupt climate changes.

[Jang et al. \(2025, this VSI\)](#) reconstruct the oceanographic history of the Sea of Japan since MIS 5 using three sediment cores. Detrital Nd isotopes indicate a reduced Tsushima Warm Current inflow during the last glacial period, linked to global sea-level lowering. This reduction led to surface water freshening, as evidenced by decreasing oxygen isotope values. Authigenic Nd data further indicate that the freshening resulted in strong stratification below 800 m, leading to oxygen-depleted bottom waters. This study emphasizes the distinctive oceanographic response of the Sea of Japan to climate-driven sea-level fluctuations and highlights its potential role as a significant global carbon reservoir during glacial periods.

[Razjigaeva et al. \(2025, this VSI\)](#) reconstruct the history of extreme flood events in western Sakhalin using peat bog stratigraphy over the past 6370 years. Based on ash content, they identified 38 flood layers. Periods of frequent extreme floods occurred during 6470–5490 a BP and 4300–3670 a BP, while severe flooding events became rare over the past 3110 years. The study suggests that strong paleotyphoons, deep extratropical cyclones, and variations in the strength of the Kuroshio Current were the primary drivers of extreme flood events during the Holocene.

[Gorbarenko et al. \(2025, this VSI\)](#) reconstructed the paleoceanographic history of the Kamchatka region from the Last Glacial Maximum (LGM) to the Holocene using microfossil and geochemical proxies. The results indicate intensified sea ice formation during the LGM and Heinrich Stadial 1. A rapid sea ice retreat occurred during the Bølling warming period, accompanied by reduced North Pacific Intermediate Water formation and the shoaling of North Pacific deep water, which brought nutrient- and CO₂-rich waters to the surface. The Holocene period was marked by four centennial-scale cold events. The study highlights the dynamic interactions among the cryosphere, ocean, and ecosystem in Northeastern Asia during the last deglaciation.

[Li et al. \(2025b, this VSI\)](#) develop a novel sedimentological proxy to reconstruct Holocene sea ice rafting in the Laptev Sea using two sediment cores. They identified a distinctive pattern of increasing coarse fraction content coupled with negative grain-size skewness as a reliable indicator of sea ice. Application of this proxy reveals that sea ice rafting initiated at 6700 cal a BP in central shelf regions and 4300 cal a BP near the Lena River estuary. Peak sea ice contributions correspond to

relatively warm intervals, suggesting complex atmosphere-ice-ocean interactions. This study provides a methodological advance in distinguishing sea ice-derived sediments from other coarse sediments in the Arctic shelf settings.

2.4. Organic carbon burial in the Asian Continental Margin and the global carbon cycle

The Asian continental margin is a typical zone of land–ocean interaction and an important region for organic carbon burial. Carbon sequestration in their margin settings plays a crucial role in the global carbon cycle and provides insights into the mechanisms of regional climate response ([Bauer et al., 2013; Shi et al., 2024](#)). Investigating the coupling between sedimentary carbon and climate change through sedimentary records helps to elucidate how climate variability and sea-level changes regulate carbon sinks on geological timescales. In this special issue, four articles focus on the burial of sedimentary organic carbon on the Arctic shelf, the eastern Chinese continental shelf, and the northeastern Indian Ocean shelf.

[Zhang et al. \(2024, this VSI\)](#) investigate the burial of terrigenous organic carbon (OCterr) in the East China Sea since the last deglaciation, based on analyses of core ECMZ. Combining TOC, TN and δ¹³C data, they find that OCterr accounts for up to 80 % of the total sedimentary organic carbon. The burial of OCterr is primarily controlled by depositional environments and the intensity of the East Asian Summer Monsoon, with stronger monsoons enhancing terrestrial input via the Changjiang River. During cold periods, the proportion of OCterr increases, likely reflecting the influence of the East Asian winter monsoon. The estimated average OCterr burial flux since 17.5 ka is approximately 3 × 10³ t C km⁻² a⁻¹, underscoring the ECS as a significant regional carbon sink.

[Zhang et al. \(2025a, this VSI\)](#) analyze Holocene fire dynamics in the Yellow River Basin using black carbon and polycyclic aromatic hydrocarbons (PAHs) preserved in sediment core YS-A from the South Yellow Sea. The results reveal an intensification of fire activity between 7.0 and 4.0 ka BP, peaking during 4.0–3.5 ka BP, followed by a decline from 3.5 to 0.5 ka BP, and a sharp resurgence after 0.5 ka BP. Climate conditions primarily governed fire frequency and intensity, while human deforestation (reducing fuel availability) and coal combustion introduced additional complexity during the late Holocene.

[Ye et al. \(2024, this VSI\)](#) investigate organic carbon (OC) burial dynamics on the Chukchi Shelf margin based on geochemical and sedimentological analyses of core LV77-3. Their results reveal clear partitioning between terrestrial and marine OC in the water column, resulting in distinct deposition patterns. Rapidly settling marine OC is preferentially buried in canyons and along shelf margins, while terrestrial OC undergoes substantial degradation during transit to the Canada Basin. The study suggests that rising Arctic marine productivity may enhance carbon sequestration, although long-term burial efficiency remains higher for terrestrial OC.

[Bai et al. \(2025, this VSI\)](#) investigate terrestrial organic carbon (OCterr) burial in the Gulf of Thailand since the last deglaciation, using geochemical proxies from sediment core T93. The multi-proxy approach combines AMS ¹⁴C dating, TOC/TN ratios, δ¹³C, and n-alkane biomarkers to identify three depositional stages. Results show that OCterr dominated during glacial lowstands with inputs from herbaceous plants, peaked during the Younger Dryas, and became modulated by monsoon-driven sedimentation during highstands. The study highlights how sea-level-controlled topography and Asian summer monsoon rainfall together influenced OCterr transport and burial in this tropical shelf system.

3. Concluding remarks

Sedimentary records from the Asian continental margin provide significant information for understanding paleoclimate and

paleoenvironmental changes throughout geological history. This special issue presents a collection of multidisciplinary and integrative studies, including sedimentology, geochemistry, mineralogy, and paleontology, based on sedimentary archives from the continental margins of the Arctic Ocean, western Pacific, and northeastern Indian Ocean. These studies shed light on source-to-sink processes and reveal the mechanisms driving multi-timescale paleoclimatic evolution along the Asian continental margin since the Neogene. Future research will focus on key regions of the Asian continental margin and promote extensive international collaboration to explore further the connection between sedimentary records and global climate change. Such efforts will enhance our understanding of the unique role of the Asian continental margin in the source-to-sink system and its broader contributions to global climate change research.

CRediT authorship contribution statement

Zhengquan Yao: Conceptualization. **Shuqing Qiao:** Conceptualization. **Christophe Colin:** Conceptualization. **Yusuke Okazaki:** Conceptualization. **Yanguang Dou:** Conceptualization.

Declaration of competing interest

The authors declare that they have no competing financial interests or personal relationships that could have appeared to influence the research reported in this paper.

Data availability

No data was used for the research described in the article.

Acknowledgements

As guest editors of this special issue, we acknowledge Editors-in-Chief, Prof. Howard Falcon-Lang and Prof. Mary Elliot for their suggestions and editorial work on this special issue. We thank all authors for their great contributions to this special issue and the reviewers who spared their valuable time to provide critical and insightful comments. This research was supported by the National Key Research and Development Program of China (2023YFF0804600).

References

- Ahagon, N., Ohkouchi, N., Uchida, M., Kawahata, H., 2003. Changes in the biological pump and ventilation in the northwestern North Pacific during the last 25,000 years. *Geophys. Res. Lett.* 30 (5), 1251. <https://doi.org/10.1029/2002GL016382>.
- An, Z., Wu, G., Li, J., Sun, Y., Liu, Y., Zhou, W., Cai, Y., Duan, A., Li, L., Mao, J., Cheng, H., Shi, Z., Tan, L., Yan, H., Ao, H., Chang, H., Juan, F., 2015. Global monsoon dynamics and climate change. *Annu. Rev. Earth Planet. Sci.* 43, 29–77. <https://doi.org/10.1146/annurev-earth-060313-054623>.
- Bai, Y., Hu, L., Jin, L., Qiao, S., Zhang, Y., Wu, B., Fan, D., Liu, S., Yang, G., Liu, J., Kornkanitnan, N., Khokatiwitong, S., Shi, X., 2025. Burial records of terrestrial organic carbon controlled by sea-level and monsoon variability in the Gulf of Thailand since the last deglaciation. *Palaeogeogr. Palaeoclimatol. Palaeoecol.* 667, 112863. <https://doi.org/10.1016/j.palaeo.2025.112863>.
- Bauer, J.E., Cai, W.J., Raymond, P.A., Bianchi, T., Hopkinson, C., Regnier, P., 2013. The changing carbon cycle of the coastal ocean. *Nature* 504, 61–70. <https://doi.org/10.1038/nature12857>.
- Cao, K., Chen, L., Lu, Y., Zhang, Y., Li, M., Wu, D., Wang, Y., Chen, L., Zhang, X., Yang, R., Huang, Y., Zhou, A., 2024. Natural and anthropogenic forcing of ecological and environmental changes at Lake Qiliu, SW China, since the last deglaciation. *Palaeogeogr. Palaeoclimatol. Palaeoecol.* 655, 112514. <https://doi.org/10.1016/j.palaeo.2024.112514>.
- Clemens, S.C., Prell, W.L., Murray, D.W., 1991. Forcing mechanisms of the Indian Ocean monsoon. *Nature* 353, 720–725. <https://doi.org/10.1038/353720a0>.
- Clift, P.D., Wan, S., Blusztajn, J., 2014. Reconstructing chemical weathering, physical erosion and monsoon intensity since 25Ma in the northern South China Sea: a review of competing proxies. *Earth Sci. Rev.* 130, 86–102. <https://doi.org/10.1016/j.earscirev.2014.01.002>.
- Cong, J., Fan, H., Bi, S., Mei, X., Dou, Y., Wang, Z., Ning, Z., Zhang, Y., 2025. The climate-driven mechanisms of sedimentary evolution in the mud area southwest off Cheju Island during the Holocene. *Palaeogeogr. Palaeoclimatol. Palaeoecol.* 676, 113127. <https://doi.org/10.1016/j.palaeo.2025.113127>.
- Dang, H., Ren, Y., Peng, N., Ma, X., Liu, F., Luo, L., Wang, Y., Jian, Z., 2024. Long-term changes in the Western Pacific warm Pool upper-water structure over the last 4 Ma. *Palaeogeogr. Palaeoclimatol. Palaeoecol.* 651, 112396. <https://doi.org/10.1016/j.palaeo.2024.112396>.
- de Vernal, A., Hillaire-Marcel, C., Le Duc, C., Roberge, P., Brice, C., Matthiessen, J., Spielhagen, R.F., Stein, R., 2020. Natural variability of the Arctic Ocean sea ice during the present interglacial. *Proc. Natl. Acad. Sci.* 117, 26069–26075. <https://doi.org/10.1073/pnas.2008996117>.
- Deemuenvai, J., Liu, Z., Zhao, Y., Shu, W., Huang, B., 2025. Early-middle Miocene deep-water circulation intensity in the South China Sea: evidence from a sortable silt record of oceanic red beds (IODP Expedition 367 Site U1500). *Palaeogeogr. Palaeoclimatol. Palaeoecol.* 659, 112664. <https://doi.org/10.1016/j.palaeo.2024.112664>.
- Dou, R., Zou, J., Dong, Z., Shi, X., Wu, Y., Zhu, A., Feng, X., Zou, X., Gorbarenko, S.A., Vasilenko, Y.P., Bosin, A.A., 2025. The impacts of Tsushima warm current and sea-ice on hydrodynamics in the Sea of Japan during the last deglaciation. *Palaeogeogr. Palaeoclimatol. Palaeoecol.* 662, 112776. <https://doi.org/10.1016/j.palaeo.2025.112776>.
- Du, S., Xiang, R., Su, X., Liu, J., Liu, S., Pan, Z., Luo, C., Zhong, F., Fang, L., 2025. Provenance and environmental changes recorded in Holocene sediments from the Southern Yellow Sea, China. *Palaeogeogr. Palaeoclimatol. Palaeoecol.* 667, 112861. <https://doi.org/10.1016/j.palaeo.2025.112861>.
- Dyke, A.S., Andrews, J.T., Clark, P.U., England, J.H., Miller, G.H., Shaw, J., Veillette, J. J., 2002. The Laurentide and Innuitian ice sheets during the last Glacial Maximum. *Quat. Sci. Rev.* 21, 9–31. [https://doi.org/10.1016/S0277-3791\(01\)00095-6](https://doi.org/10.1016/S0277-3791(01)00095-6).
- Fernandes, M.C., Sebastian, T., Vadakkepuliyambatta, S., Nayak, P., Yadava, M.G., Kurian, P.J., 2025. Organic matter sources and productivity variations in the southeastern Bay of Bengal in the past 54,000 years. *Palaeogeogr. Palaeoclimatol. Palaeoecol.* 670, 112970. <https://doi.org/10.1016/j.palaeo.2025.112970>.
- Gorbarenko, S.A., Shi, X., Bosin, A.A., Liu, Y., Vasilenko, Y.P., Yanchenko, E.A., Derkachev, A.N., Kirchenko, I.S., Artemova, A.V., Velivetskaya, T.A., Psheneva, O. Y., 2024. Millennial-scale changes in the environment, ice conditions, and deep-water ventilation at the Detroit-Tenji Seamounts, Northwest Pacific, over the last 43 kyr. *Quat. Sci. Rev.* 325. <https://doi.org/10.1016/j.quascirev.2023.108472>.
- Gorbarenko, S.A., Artemova, A.V., Psheneva, O.Y., Vagina, N.K., Shi, X., Bosin, A.A., Vasilenko, Y.P., Yao, Z., Liu, Y., Yanchenko, E.A., Novoselova, Y.V., Zou, J., 2025. Orbital-millennial-centennial evolution of paleceanography and sea ice in the northwestern Pacific during the LGM-Holocene inferred from micropaleontological, geochemical and lithological proxies. *Palaeogeogr. Palaeoclimatol. Palaeoecol.* 667, 112862. <https://doi.org/10.1016/j.palaeo.2025.112862>.
- Huang, P., Hu, N., Shi, X., Li, A., Liu, J., 2025. Impact of continental weathering on deep northwestern Pacific eNd over the past 16,000 years. *Palaeogeogr. Palaeoclimatol. Palaeoecol.* 661, 112710. <https://doi.org/10.1016/j.palaeo.2024.112710>.
- Jakobsson, M., Andreassen, K., Bjarnadóttir, L.R., Dove, D., Dowdeswell, J.A., England, J.H., Funder, S., Hogan, K., Ingólfsson, Ó., Jennings, A., Krog Larsen, N., Kirchner, N., Landvik, J.Y., Mayer, L., Mikkelsen, N., Möller, P., Niessen, F., Nilsson, J., O'Regan, M., Polyak, L., Nørgaard-Pedersen, N., Stein, R., 2014. Arctic Ocean glacial history. *Quat. Sci. Rev.* 92, 40–67. <https://doi.org/10.1016/j.quascirev.2013.07.033>.
- Jakobsson, M., Nilsson, J., Anderson, L., Backman, J., Bjork, G., Cronin, T.M., Kirchner, N., Koschurnikov, A., Mayer, L., Noormets, R., O'Regan, M., Stranne, C., Ananiev, R., Barrientos Macho, N., Cherniykh, D., Coxall, H., Eriksson, B., Floden, T., Gemery, L., Gustafsson, O., Jerram, K., Johansson, C., Khorov, A., Mohammad, R., Semiletov, I., 2016. Evidence for an ice shelf covering the Central Arctic Ocean during the penultimate glaciation. *Nat. Commun.* 7, 10365. <https://doi.org/10.1038/ncomms10365>.
- Jang, K., Bayon, G., Han, Y., Ahn, Y., Joe, Y.J., Son, Y.J., Lee, S., Jin, J.H., Byun, E., Nam, S.-I., 2025. Paleceanographic responses to sea level variability in the East Sea since the last glacial period: Multi-proxy approach. *Palaeogeogr. Palaeoclimatol. Palaeoecol.* 661, 112706. <https://doi.org/10.1016/j.palaeo.2024.112706>.
- Kinnard, C., Zdanowicz, C.M., Fisher, D.A., Isaksson, E., de Vernal, A., Thompson, L.G., 2011. Reconstructed changes in Arctic sea ice over the past 1,450 years. *Nature* 479 (7374), 509–512. <https://doi.org/10.1038/nature10581>.
- Knies, J., Kleiber, H.-P., Matthiessen, J., Müller, C., Nowaczyk, N., 2001. Marine ice rafted debris records constrain maximum extent of Saalian and Weichselian ice-sheets along the northern Eurasian margin. *Glob. Planet. Chang.* 31, 45–64. [https://doi.org/10.1016/S0921-8181\(01\)00112-6](https://doi.org/10.1016/S0921-8181(01)00112-6).
- Li, F., Yang, S., Breecker, D.O., Guo, Y., Ramos, E.J., Huang, X., Deng, K., Yu, J., Li, S., 2024a. Large river expansion and global cooling controlled the Plio-Pleistocene weathering intensity records in East Asian margin. *Palaeogeogr. Palaeoclimatol. Palaeoecol.* 655, 112517. <https://doi.org/10.1016/j.palaeo.2024.112517>.
- Li, G., Xia, G., Ji, C., Wagreich, M., Ogg, J.G., Yi, H., 2024b. Late Jurassic paleoenvironmental reconstruction based on stable oxygen isotopes in bulk carbonates from the Qiangtang Basin, eastern Tethys. *Palaeogeogr. Palaeoclimatol. Palaeoecol.* 655, 112525. <https://doi.org/10.1016/j.palaeo.2024.112525>.
- Li, J., Shi, X., Liu, S., Li, F., Miao, X., Jiang, R., Khokatiwitong, S., Kornkanitnan, N., 2024c. Sensitive response of erosion and weathering to the Indian Summer Monsoon changes in South Asia during Dansgaard-Oeschger oscillations. *Palaeogeogr. Palaeoclimatol. Palaeoecol.* 655, 112516. <https://doi.org/10.1016/j.palaeo.2024.112516>.
- Li, X.-M., Chen, J.-Y., Cao, Z.-D., Liu, L.-M., Zhang, S.-H., Zhang, Y.-Z., Wei, L.-J., Xie, S.-P., 2024d. Miocene evolution of vegetation, climate, and elevation in the Wulan Basin of northeast Tibetan Plateau based on a CRACLE analysis of palynological assemblages. *Palaeogeogr. Palaeoclimatol. Palaeoecol.* 656, 112563. <https://doi.org/10.1016/j.palaeo.2024.112563>.

- Li, P., Yang, S., Luo, Y., Liu, L., Zhang, Y., Liu, W., Zhang, J., Xu, X., Wen, C., Li, Q., 2025a. Indian summer monsoon history during the last glacial cycle revealed by a loess sequence from the Tibetan Plateau. *Palaeogeogr. Palaeoclimatol. Palaeoecol.* 657, 112593. <https://doi.org/10.1016/j.palaeo.2024.112593>.
- Li, Q., Qiao, S., Shi, X., Hu, L., Yu, Y., Bosin, A., Vasilenko, Y., Feng, H., Dong, J., Jin, L., Ye, X., Qi, Y., 2025b. Sedimentary record of sea ice rafting in the Laptev Sea during the Holocene: evidence from the improved ice rafting debris (IRD) proxy. *Palaeogeogr. Palaeoclimatol. Palaeoecol.* 660, 112667. <https://doi.org/10.1016/j.palaeo.2024.112667>.
- Liang, J., Wang, Y., Zhang, S., Huang, C., Xu, E., Zhang, Z., 2025. Astronomical Forcing of late oligocene to early Miocene Paleoclimate: a case study from the Northern South China Sea. *Palaeogeogr. Palaeoclimatol. Palaeoecol.* 673, 113007. <https://doi.org/10.1016/j.palaeo.2025.113007>.
- Li, P., Zhang, J., Liu, Y., Sun, Q., Zhang, D., Li, Y., Wei, T., Yu, J., Wang, J., Chen, J., 2024. Sediment source-to-sink patterns along the Southeast China coast during the late Quaternary: New insights from sediment geochemistry and OSL ages in Ningde Bay. *Palaeogeogr. Palaeoclimatol. Palaeoecol.* 656, 112577. <https://doi.org/10.1016/j.palaeo.2024.112577>.
- Li, S., Liu, Y., Shan, X., Hu, W., Zhao, N., Wang, Y.P., Feng, W., Chen, Y., Wang, X., Feng, A., 2025. Evolution of multiple peat beds in postglacial transgressive deposits of western Bohai Sea and their paleoenvironmental implications. *Palaeogeogr. Palaeoclimatol. Palaeoecol.* 660, 112709. <https://doi.org/10.1016/j.palaeo.2024.112709>.
- Lu, J., Zhang, H., Zhang, R., Cui, J., Bao, Y., Niu, X., Cai, Y., Cheng, H., 2025. Early-Middle Holocene climate change and its impact on the succession of Neolithic cultures in southern Hangzhou Bay. *Palaeogeogr. Palaeoclimatol. Palaeoecol.* 659, 112652. <https://doi.org/10.1016/j.palaeo.2024.112652>.
- McManus, J.F., Francois, R., Gherardi, J.M., Keigwin, L.D., Brown-Leger, S., 2004. Collapse and rapid resumption of Atlantic meridional overturning circulation at the end of the last glacial period. *Nature* 428 (6985), 834–837. <https://doi.org/10.1038/nature02494>.
- Mohanty, S., Chaudhuri, S., Chattopadhyay, K., Patrick, N.M., Vats, N., Bhaumik, A.K., 2025. Influence of monsoon variability on hydrographic and productivity dynamics in the western Bay of Bengal during the late Holocene: a planktic foraminiferal perspective. *Palaeogeogr. Palaeoclimatol. Palaeoecol.* 670, 112971. <https://doi.org/10.1016/j.palaeo.2025.112971>.
- Niu, Y., Qi, L., Qiao, Y., 2024. Quaternary provenance changes in the loess deposits of the western Chinese Loess Plateau: Insights from U-Pb age spectra of detrital zircon. *Palaeogeogr. Palaeoclimatol. Palaeoecol.* 655, 112498. <https://doi.org/10.1016/j.palaeo.2024.112498>.
- Novoselova, Y.V., Gorbarenko, S.A., Shi, X., Bosin, A.A., Liu, Y., 2025. Millennial-scale vegetation and climate changes in the Sea of Japan region over the last 120 kyr inferred from marine sediments. *Palaeogeogr. Palaeoclimatol. Palaeoecol.* 667, 112892. <https://doi.org/10.1016/j.palaeo.2025.112892>.
- Peng, H., Zheng, Y., Zhou, M., Wang, Y., Ran, L., Jiang, H., Pérez-Cruz, L., Venegas, R., Höfig, T., Teske, A., Lizarralde, D., Marsaglia, K., Cui, Y., Jiang, S., 2025. Climate change regulated carbonate production and accumulation in the Guaymas Basin over the past ca. 450,000 years. *Palaeogeogr. Palaeoclimatol. Palaeoecol.* 666, 112864. <https://doi.org/10.1016/j.palaeo.2025.112864>.
- Pi, Z., Chang, F., Nan, Q., Cui, Y., Liu, Q., Zhang, J., Li, H., Chen, J., Li, T., 2024. The evolution and relationship of the Yellow Sea warm current and the Yellow Sea Cold Water Mass since the Mid-Holocene and possible ENSO influences. *Palaeogeogr. Palaeoclimatol. Palaeoecol.* 655, 112494. <https://doi.org/10.1016/j.palaeo.2024.112494>.
- Prell, W.L., Kutzbach, J.E., 1987. Monsoon variability over the past 150,000 years. *J. Geophys. Res.* 92, 8411–8425. <https://doi.org/10.1029/JD092iD07p08411>.
- Rae, J.W.B., Gray, W.R., Wills, R.C.J., Eisenman, I., Fitzhugh, B., Fotheringham, M., Littley, E.F.M., Rafter, P.A., Rees-Owen, R., Ridgwell, A., Taylor, B., Burke, A., 2020. Overturning circulation, nutrient limitation, and warming in the Glacial North Pacific. *Sci. Adv.* 6. <https://doi.org/10.1126/sciadv.abd1654>.
- Rahman, A., Wang, L.-C., 2025. Hydroclimate changes in northern Taiwan during 13.3 cal kyr BP through the Tsui Tsui Valley sediments. *Palaeogeogr. Palaeoclimatol. Palaeoecol.* 663, 112775. <https://doi.org/10.1016/j.palaeo.2025.112775>.
- Razjigavaeva, N.G., Ganzev, L.A., Grebennikova, T.A., Ponomarev, V.I., Afanasyev, V.V., Gorbunov, A.O., Klimin, M.A., 2025. Extreme flood events on Western Sakhalin and their linkage to cyclogenesis activity in the western North Pacific in middle-late Holocene. *Palaeogeogr. Palaeoclimatol. Palaeoecol.* 669, 112933. <https://doi.org/10.1016/j.palaeo.2025.112933>.
- Shi, X., Wu, B., Qiao, S., Yao, Z., Hu, L., Bai, Y., Hu, S., Sheng, J., Liu, Y., Liu, S., Wang, K., Zou, J., 2024. Distribution, burial fluxes and carbon sink effect of sedimentary organic carbon in the eastern China seas. *Sci. China Earth Sci.* 67, 3062–3082. <https://doi.org/10.1007/s11430-024-1412-0>.
- Song, Z., Wan, S., Yu, Z., Yu, M., Colin, C., Tang, Y., Zhang, J., Jin, H., Zhao, D., Shi, X., Li, A., 2024. The major uplift in Himalayas was no earlier than the Miocene: evidence from marine sediment record in the Bay of Bengal. *Palaeogeogr. Palaeoclimatol. Palaeoecol.* 648, 112275. <https://doi.org/10.1016/j.palaeo.2024.112275>.
- Stein, R., Fahl, K., Gierz, P., Niessen, F., Lohmann, G., 2017. Arctic Ocean sea ice cover during the penultimate glacial and the last interglacial. *Nat. Commun.* 8, 373. <https://doi.org/10.1038/s41467-017-00552-1>.
- Tang, N., Wang, Z., Lin, P., Liu, Y., Wu, Z., Tian, H., Mei, X., Sun, J., Qi, J., Li, R., Wu, S., Chu, H., Lai, Z., 2025. Luminescence dating of core DLC70-2 from the North Yellow Sea in China and its implication for late Quaternary transgressions. *Palaeogeogr. Palaeoclimatol. Palaeoecol.* 666, 112842. <https://doi.org/10.1016/j.palaeo.2025.112842>.
- Thena, T., Nair, N., Pandey, D.K., 2025. Benthic Foraminiferal recovery following a massive Submarine Landslide in the Laxmi Basin, Arabian Sea (IODP U1457). *Palaeogeogr. Palaeoclimatol. Palaeoecol.* 676, 113150. <https://doi.org/10.1016/j.palaeo.2025.113150>.
- Wang, A., Yao, Z., Shi, X., Wang, K., Zou, J., Liu, Y., Wu, Y., Gorbarenko, S.A., 2021. Orbital and Millennial Variations in Sea Ice in the Southwestern Okhotsk Sea since the last Interglacial Period and their Implications. *Front. Earth Sci.* 9. <https://doi.org/10.3389/feart.2021.710797>.
- Wang, L., Deng, H., Zhao, H., Xia, H., Zhou, A., Wang, Q., Chen, F., 2024. Effect of plant roots on the radiocarbon age of loess deposits in arid Central Asia. *Palaeogeogr. Palaeoclimatol. Palaeoecol.* 651, 112403. <https://doi.org/10.1016/j.palaeo.2024.112403>.
- Wu, S., Liu, J., Chu, H., Feng, Y., Yin, M., Pei, L., 2024. Paleoenvironmental evolution and East Asian monsoon records through three stages of paleochannels since the mid-Pleistocene in the western Bohai Sea, North China. *Palaeogeogr. Palaeoclimatol. Palaeoecol.* 656, 112603. <https://doi.org/10.1016/j.palaeo.2024.112603>.
- Wu, F., Jian, Z., Xie, X., Coletti, G., Zhu, Y., Shang, Z., Chen, B., 2025. Late Miocene carbonate-system evolution in the Xisha area, northern South China Sea. *Palaeogeogr. Palaeoclimatol. Palaeoecol.* 665, 112812. <https://doi.org/10.1016/j.palaeo.2025.112812>.
- Xiao, J., Song, Y., Ning, Q., Sun, H., Li, Y., Yu, S., Liu, H., 2025. Stepwise evolution of the Weihe Basin since the late Pliocene and implications for Yellow River development. *Palaeogeogr. Palaeoclimatol. Palaeoecol.* 661, 112721. <https://doi.org/10.1016/j.palaeo.2025.112721>.
- Xiong, W., Huang, L., Zhang, Y., Wang, Z., Bi, N.S., Pan, J., Sun, J., He, L., Wang, F., Mei, X., 2025. Quaternary transgression process controlled by tectonic subsidence over the last 1.35 Ma: New insights from the eastern Bohai Sea. *Palaeogeogr. Palaeoclimatol. Palaeoecol.* 657, 112602. <https://doi.org/10.1016/j.palaeo.2024.112602>.
- Xu, T., Liu, X., Fang, X., Zhu, A., He, L., Wang, H., Chen, J., Xiong, Z., Liu, Y., Shi, X., 2024. Sedimentary evolution of the Holocene subaqueous Changjiang Delta, with an emphasis on contributions of the two major Rivers, the Changjiang and Yellow Rivers. *Palaeogeogr. Palaeoclimatol. Palaeoecol.* 655, 112501. <https://doi.org/10.1016/j.palaeo.2024.112501>.
- Xu, F., Zhang, X., Xu, J., Sun, Z., Yuan, S., Liu, X., 2025a. Sea level and low-latitude climate control on sedimentary provenance and paleoenvironmental evolution in the Central Okinawa Trough since 19 cal. ka BP. *Palaeogeogr. Palaeoclimatol. Palaeoecol.* 658, 112621. <https://doi.org/10.1016/j.palaeo.2024.112621>.
- Xu, X., Qiang, X., Li, X., Qiu, H., Zhao, H., Fu, C., Yang, Z., 2025b. Magnetic proxy in the Heqing drill core revealed Indian Summer Monsoon variations linked with AMOC at the orbital-scale during the late Pleistocene. *Palaeogeogr. Palaeoclimatol. Palaeoecol.* 665, 112814. <https://doi.org/10.1016/j.palaeo.2025.112814>.
- Ye, L., Yu, X., Liu, Y., Astakhov, A.S., Bosin, A., Bian, Y., Dong, L., Fan, W., Yang, H., 2024. Organic carbon burial dynamics at the Chukchi Shelf margin: Implications for the Arctic Ocean carbon sink. *Palaeogeogr. Palaeoclimatol. Palaeoecol.* 655, 112534. <https://doi.org/10.1016/j.palaeo.2024.112534>.
- Ye, M., Zhu, Y., Shao, L., Fan, H., Liu, P., Xie, X., 2025. Carbonate beach-ridge deposits on SD island, Xisha Islands: Implications for paleostorms events during MIS 5. *Palaeogeogr. Palaeoclimatol. Palaeoecol.* 661, 112720. <https://doi.org/10.1016/j.palaeo.2025.112720>.
- Yu, S., Chen, F., Huang, K., Zhou, Y., Zhu, Q., Wu, C., Zhuang, C., Cao, K., Yamin, L., Zhang, J., Zheng, Z., 2025. The vegetation response to MIS5 and MIS1 as revealed by pollen data from the Pearl River estuary, China. *Palaeogeogr. Palaeoclimatol. Palaeoecol.* 662, 112774. <https://doi.org/10.1016/j.palaeo.2025.112774>.
- Yuan, W., Liu, B., Wu, Z., Wang, Y., Sun, Z., Zhou, X., Tian, R., Yan, B., Lai, Z., 2025. Luminescence dating of core sediments from Jining of Shandong Province in the lower Yellow River Plain and its geomorphological implications. *Palaeogeogr. Palaeoclimatol. Palaeoecol.* 675, 113042. <https://doi.org/10.1016/j.palaeo.2025.113042>.
- Yue, W., Yang, S., Yue, X., Zhao, B., Huang, X., Zhang, L., Li, Y., Chen, J., Chen, Z., 2024. Fingerprint of Plio–Quaternary detrital zircon geochronology: implications for sediment provenances and geomorphological evolution of the Yangtze Delta. *Palaeogeogr. Palaeoclimatol. Palaeoecol.* 655, 112552. <https://doi.org/10.1016/j.palaeo.2024.112552>.
- Zhang, M., Liu, X., Li, A., Chang, X., Hu, L., Bi, N., Zhuang, G., Wang, H., 2024. Fate of terrigenous organic carbon within shelf sediments from the East China Sea controlled by sea-level and climatic changes since the last deglaciation. *Palaeogeogr. Palaeoclimatol. Palaeoecol.* 650, 112386. <https://doi.org/10.1016/j.palaeo.2024.112386>.
- Zhang, C., Qiu, Y., Wang, C., Fan, Q., Feng, Z., Zou, X., 2025a. Pyrogenic carbon records of Holocene fire dynamics in the Yellow River Basin: climate change and human activity forcing. *Palaeogeogr. Palaeoclimatol. Palaeoecol.* 659, 112626. <https://doi.org/10.1016/j.palaeo.2024.112626>.
- Zhang, J., Liu, J., Zhang, X., Yue, B., Qiu, J., 2025b. Mineralogy of the Yangtze (Changjiang) shoal: Implications for provenance and land-sea interaction response to sea level changes since MIS 6. *Palaeogeogr. Palaeoclimatol. Palaeoecol.* 664, 112813. <https://doi.org/10.1016/j.palaeo.2025.112813>.
- Zhang, J., Lv, D., Yu, M., Zhuo, Z., Liu, X., Liu, Y., Zhang, H., Liu, B., Qiang, X., Kang, S., Sun, Y., 2025c. High-resolution elemental compositions of fluvial deposits in the Eastern Henan Basin and its implications for climatic variability over the last 3.5 Ma. *Palaeogeogr. Palaeoclimatol. Palaeoecol.* 675, 113043. <https://doi.org/10.1016/j.palaeo.2025.113043>.
- Zhang, L., Liu, Y., Bai, M., Hao, Z., 2025d. Solar modulation of hydroclimatic patterns in eastern China under influences of the Pacific Decadal Oscillation and Atlantic Multidecadal Oscillation. *Palaeogeogr. Palaeoclimatol. Palaeoecol.* 663, 112796. <https://doi.org/10.1016/j.palaeo.2025.112796>.

- Zhang, X., Zhou, X., Tan, G., Huang, S., Shan, X., Lin, C., Zhang, X., 2025e. Sea-level and climatic evolution in the postglacial Qiantang River incised-valley system: Insights from grain-size end-member modeling and geochemical characteristics. *Palaeogeogr. Palaeoclimatol. Palaeoecol.* 661, 112707. <https://doi.org/10.1016/j.palaeo.2024.112707>.
- Zhang, Y., Zheng, S., Yao, H., Xu, Y., Yi, L., Li, D., Ye, Y., Liu, S., Zhang, Y., Xue, L., 2025f. Sedimentary records of the southern Taiwan Strait since the late Pliocene and implications for sea-level and tectonic changes. *Palaeogeogr. Palaeoclimatol. Palaeoecol.* 663, 112797. <https://doi.org/10.1016/j.palaeo.2025.112797>.
- Zheng, H., Jiang, F., Yan, Y., Feng, X., Xiong, Z., Jia, Q., Qin, B., Ren, C., Xu, Z., Li, T., 2025. Intertropical Convergence Zone modulates Asian dust input to the low-latitude western Pacific during the late Neogene. *Palaeogeogr. Palaeoclimatol. Palaeoecol.* 675, 113074. <https://doi.org/10.1016/j.palaeo.2025.113074>.